

A city-scale roof shape classification using machine learning for solar energy applications

Nahid Mohajeri ^{a,b,*}, Dan Assouline ^a, Berenice Guiboud ^a, Andreas Bill ^a, Agust Gudmundsson ^c, Jean-Louis Scartezzini ^a

^a Solar Energy and Building Physics Laboratory (LESO-PB), Ecole Polytechnique Fédérale de Lausanne (EPFL), 1015, Lausanne, Switzerland

^b Sustainable Urban Development Programme, Department for Continuing Education, University of Oxford, Rewley House, 1 Wellington Square, Oxford, OX1 2JA, United Kingdom

^c Department of Earth Sciences, Royal Holloway University of London, Egham, TW20 0EX, United Kingdom



ARTICLE INFO

Article history:

Available online 28 December 2017

Keywords:

Machine learning
Roof shape classification
PV potential
Support Vector Machine

ABSTRACT

Solar energy deployment through PV installations in urban areas depends strongly on the shape, size, and orientation of available roofs. Here we use a machine learning approach, Support Vector Machine (SVM) classification, to classify 10,085 building roofs in relation to their received solar energy in the city of Geneva in Switzerland. The SVM correctly identifies six types of roof shapes in 66% of cases, that is, flat & shed, gable, hip, gambrel & mansard, cross/corner gable & hip, and complex roofs. We classify the roofs based on their useful area for PV installations and potential for receiving solar energy. For most roof shapes, the ratio between useful roof area and building footprint area is close to one, suggesting that footprint is a good measure of useful PV roof area. The main exception is the gable where this ratio is 1.18. The flat and shed roofs have the second highest useful roof area for PV (complex roof being the highest) and the highest PV potential (in GWh). By contrast, hip roof has the lowest PV potential. Solar roof-shape classification provides basic information for designing new buildings, retrofitting interventions on the building roofs, and efficient solar integration on the roofs of buildings.

© 2017 Elsevier Ltd. All rights reserved.

1. Introduction

Photovoltaics (PV) are among the most promising emerging technologies for deployment of solar energy in urban areas. Solar PV panels can be installed on the rooftops of individual buildings. They have proven to be an efficient and viable resource of sustainable renewable energy for the urban areas [1–6]. However, to reach their full potential for the urban scale many socio-technological and economical decisions need to be made. Improvements are also needed as regards urban characteristics such as design, geometry, and positioning of buildings [7]. While roofs of buildings in urban areas provide promising and increasingly important locations for PV installations, an efficient method for finding and evaluating suitable roofs on existing buildings for the optimal location of PVs remains a challenge.

There have been several studies focusing on mapping solar energy potential and feasibility of solar PV installations on building rooftops at the neighbourhood and the urban scales using different methods. For example, Wiginton et al. [1] use a sampling technique as well as the GIS-based Feature Analyst (FA) tool to estimate the rooftop PV potential. Several other studies have used aerial images and ArcGIS LiDAR data to determine roof geometries and to estimate their PV potential at a regional scale [3–6,8,9]. Assouline et al. [10] introduced a method that combines Geographic Information Systems (GIS) for data processing and a machine learning approach to estimate the building rooftop solar PV potential for cities in Switzerland. While there are many recent studies on modelling roof geometries for solar application based on simplification of roof shapes [11,12] and geo-spatial techniques [1,13,14], few studies, so far, explore the relation between roof shapes of new buildings and their solar potential with a view of providing support for design development [15–18]. Recently, machine learning algorithms (e.g. Support Vector Machines, Random Forests, Artificial Neural Networks) have been extensively used for different applications. These include forecasting solar radiation [19] as well as geospatial

* Corresponding author. Solar Energy and Building Physics Laboratory (LESO-PB), Ecole Polytechnique Fédérale de Lausanne (EPFL), 1015, Lausanne, Switzerland.

E-mail addresses: nahid.mohajeri@epfl.ch, nahid.mohajeri@conted.ox.ac.uk (N. Mohajeri).

environmental data modelling [20–22]. However, using machine learning algorithms so as to classify urban characteristics for solar applications, including impacts of different roof shapes on annual solar PV electricity production, has remained a challenge.

In the present study, we develop a novel approach using Support Vector Machine (SVM), a kernel-based machine learning technique, to classify roof shapes based on their solar PV potential. We focus on the city of Geneva in Switzerland. The city latitude is 46.2° N, the longitude is 6.15° E, and its average elevation is 374 m. Geneva, with a population of about 200 thousand in 2015 (www.bfs.admin.ch), is the second largest city in Switzerland and the largest one in the French-speaking part of the country. There are 11,806 buildings in Geneva. However, all the factors that we analyse were available for only 10,085 buildings, which is thus the number used in this study.

The main aims of this study are to: (1) explore the variability of 10,085 building roofs in the city of Geneva; (2) use a machine learning methodology to classify the building roof shapes in the city in relation to their solar potential; (3) rank the roof shapes based on their received solar energy and potential for PV electricity production; and (4) classify the building types (e.g. residential, commercial, and industry) based on the roof shape and the solar PV potential.

2. Methods and data

To classify the building roof shapes in the city of Geneva based on their solar energy potential, we use a machine learning algorithm, that is, the Support Vector Machine (SVM). SVM is one of the most efficient machine learning algorithms for classification tasks. It was first introduced by Cortes and Vapnik in 1995 [23]. Section 2.1 gives a short description of the main principles of the method. In Section 2.2, we explain briefly the data and the estimation method for yearly mean solar radiation on the rooftops. We use yearly mean solar radiation data, which is freely available for building rooftops of the city of Geneva from (<http://ge.ch/sitg/>).

2.1. Support Vector Machine for classification

Support Vector Machines (SVMs) are primarily an example of a linear classifier. They can, however, be extended to a non-linear classifier with kernel functions [20,23–27]. SVM is a machine learning technique based on the concept of decision planes (hyperplanes) which define the decision boundaries of the classifier. It was originally used to solve a binary classification problem. The principle of the algorithm for a binary classification, however, can be easily extended to a multi-class classification problem. We consider a set of training data with two classes of points C_1 and C_2 . The goal of a classification task is to design a function f that can assign any new point \mathbf{x} to either C_1 or C_2 , using the training data. One way to design such a function is to find the boundary between the classes, separating the two different classes with a linear decision surface. This is a line in 2D, a plane in 3D, or a hyperplane in higher dimensions.

The basic idea of SVM is to find the optimal separating hyperplane between the two classes (C_1 and C_2) by maximizing the margin between the closest points of the classes (Fig. 1). The points lying on the boundaries are called support vectors and the middle of the margin is defined by the optimal separating hyperplane (Fig. 1a). To start from the simplest case, suppose that this separation is possible without misclassifications. Then the data set is called linearly separable. Since real data are usually not linearly separable, this assumption is relaxed to obtain a linear classifier

that allows for classification errors and is known as a soft margin classifier.

Consider the following basic set of linear functions:

$$f(x) = \mathbf{w} \cdot \mathbf{x} + b \quad (1)$$

where \mathbf{x} is a vector in R^d (input space of dimension d), b is a scalar, and \mathbf{w} is an unknown vector in R^d , that is, a weight vector or normal (perpendicular) to the hyperplane. In a classification task, the sign of the function $f(x)$ is the output of the classifier. We consider the data to be linearly separable. Thus, it is a hyperplane that separates class C_1 from class C_2 (Fig. 1a). The hyperplane can be defined by $\mathbf{w} \cdot \mathbf{x} + b = 0$. For the hyperplane to be as far from the support vectors as possible, we need to maximize the margin. A simple computation leads to a margin of $\frac{2}{\|\mathbf{w}\|}$, where $\|\mathbf{w}\|$ is the Euclidean norm of \mathbf{w} , a measure of its length. As mentioned above, SVMs are originally a kind of linear classifier. Consider the following decision function, defined by \mathbf{w} and b [21,26,27]:

$$y = \begin{cases} +1, & \text{if } \mathbf{w} \cdot \mathbf{x} - b \geq 1 \\ -1, & \text{if } \mathbf{w} \cdot \mathbf{x} - b \leq 1 \end{cases} \quad (2)$$

Given a training data $\{(\mathbf{x}_i, y_i)\} (i = 1, 2, \dots, L)$, L is the number of training points, where $\mathbf{x}_i \in R^d$ is the input vector of dimension d (the number of features) and $y_i \in R$ is the desired output value (called the label) for point i, we impose the above decision function, Eq. (2), as a set of constraints on the training data:

$$\mathbf{w} \cdot \mathbf{x}_i + b \geq +1, \quad \text{if } y_i = +1 \quad (3)$$

$$\mathbf{w} \cdot \mathbf{x}_i + b \leq -1, \quad \text{if } y_i = -1 \quad (4)$$

The two set of equations can be combined into:

$$y_i(\mathbf{w} \cdot \mathbf{x}_i + b) \geq 1 \quad (5)$$

Equation (5) is the constraint of our optimization problem. As mentioned above, the objective is to maximize the margin $\frac{2}{\|\mathbf{w}\|}$, representing the distance between the two dashed lines in Fig. 1a, subject to the constraint in Eq. (5), which is equivalent to find:

$$\min \mathbf{w} \text{ such that } y_i(\mathbf{w} \cdot \mathbf{x}_i + b) \geq 1$$

Minimizing \mathbf{w} is equivalent to minimizing $\frac{1}{2}\|\mathbf{w}\|^2$. Using this term makes it possible to perform Quadratic Programming (QP) optimization later on. We therefore need to [21,23–27]:

$$\begin{aligned} \text{Minimize} \quad & \frac{1}{2}\|\mathbf{w}\|^2 \\ \text{subject to} \quad & y_i(\mathbf{w} \cdot \mathbf{x}_i + b) - 1 \geq 0 \end{aligned} \quad (6)$$

We use the Lagrangian formulation to solve this optimization problem. This is a general analytical method to solve constrained optimization problems. Introducing the Lagrange multipliers α_i for the constraints, one has to minimize the Lagrange functional (Lagrangian) L_P with respect to \mathbf{w} and b and maximize the Lagrangian with respect to α_i [21,26]:

$$L_P = \frac{1}{2}\|\mathbf{w}\|^2 - \sum_{i=1}^L \alpha_i y_i (\mathbf{w} \cdot \mathbf{x}_i + b) + \sum_{i=1}^L \alpha_i \quad (7)$$

subject to the following constraints:

$$\alpha_i \geq 0, \quad i = 1, 2, \dots, L \quad (8)$$

This can be done by differentiating L_P with respect to \mathbf{w} and b and setting the derivatives to zero [21,26]:

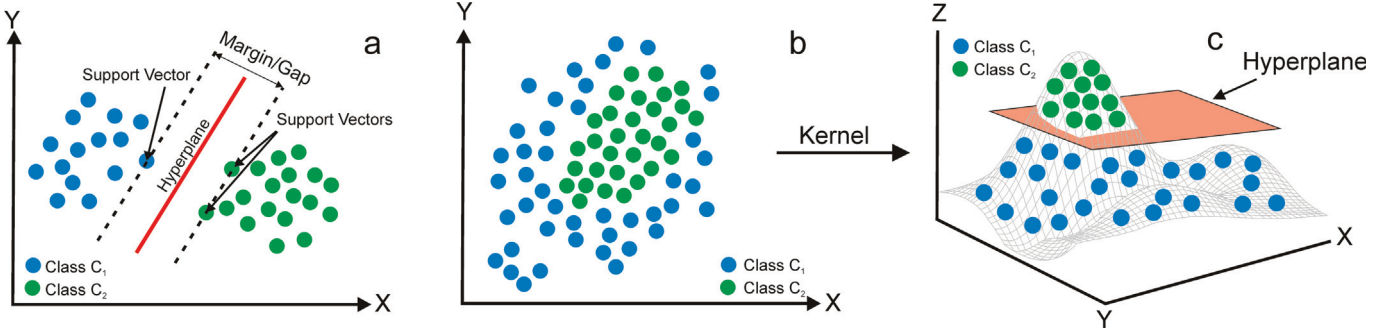


Fig. 1. A schematic graph showing the main concept of SVM for classification. (a) Hyperplane through two arbitrary linearly separable classes. (b) Two non-linearly separable classes. (c) Non-linear mapping of 2D data into 3D using kernels in which the maximum margin hyper-plane can be constructed.

$$\frac{\partial L_p}{\partial w} = 0 \Rightarrow w = \sum_{i=1}^L \alpha_i y_i x_i \quad (9)$$

$$\frac{\partial L_p}{\partial b} = 0 \Rightarrow \sum_{i=1}^L \alpha_i y_i = 0 \quad (10)$$

Substituting Eqs. (9) and (10) into Eq. (7) gives a new formula which depends on α and we need to maximize, namely [21,26]:

$$L_D = \sum_{i=1}^L \alpha_i - \frac{1}{2} \sum_{i=1}^L \sum_{j=1}^L \alpha_i \alpha_j y_i y_j x_i \cdot x_j \quad (11)$$

subject to the following constraints:

$$\sum_{i=1}^L \alpha_i y_i = 0, \alpha_i \geq 0, \quad (12)$$

here, L_D refers to as the *Dual form* of the *Primal L_p* . The Dual form requires only the dot product of each input vector x_i to be calculated, which is important for the *Kernel Trick* described in the next part. Thus, the decision function becomes:

$$f(x) = \sum_{i=1}^L y_i \alpha_i x_i \cdot x + b \quad (13)$$

This is a convex quadratic problem with respect to linear constraints which can be solved with Quadratic Programming (QP). Any well-known method can be applied to solve it [28].

In order to extend the SVM methodology to handle data that is not fully linearly separable, we relax the constraints for Eq. (5) slightly so as to allow for misclassified points. This is done by introducing positive slack variables $\xi_i \geq 0$ to the constraints (5) [23,26]:

$$y_i(w \cdot x_i + b) \geq 1 - \xi_i \quad (14)$$

As few ξ_i as possible should be non-zero. To minimize the overall error brought by the slack variables, the optimization problem becomes:

$$\text{Minimise } \frac{1}{2} \|w\|^2 + C \sum_{i=1}^L \xi_i$$

$$\text{Subject to } y_i(w \cdot x_i + b) \geq 1 - \xi_i \quad (15)$$

where the parameter C controls the trade-off between the slack variable penalty and the size of the margin. More specifically, the constant C determines the trade-off between the generalization of

the classifier and the amount of outliers tolerated (if C is too big the data will be overfitted and the capacity to adapt to a new data will be low. However, if C is too small it might adapt well but will not have enough memory of the training data to classify well). For this problem, the same approach of Lagrangian multipliers is used as for linearly separable data. However, one has to introduce the Lagrange multipliers for the constraints $\xi_i \geq 0$ as well in order to arrive at the dual formulation of the problem. The resulting optimization is also a QP-problem and can be solved by standard QP solvers. The trade-off constant C becomes an upper bound for the weights in the dual formulation, resulting in the following constraints: $0 \leq \alpha_i \leq C, i = 1, 2, \dots, L$.

To move from a linear classifier to a non-linear classifier (Fig. 1b,c), a set of mathematical functions, kernels, are defined. The performance of SVM depends heavily on the choice of the kernel function, that is, $k(x_i, x_j)$. Using the kernel function, we implicitly map the input data to a so-called feature space, where f can be defined as a linear function. We compute $k(x_i, x_j) = \langle \varphi(x_i), \varphi(x_j) \rangle$, where $k(x_i, x_j)$ is the kernel function and φ is a mapping from the original input space to the feature space [29–31]. The feature space is constructed via the projection, that is, kernel trick. Only $k(x_i, x_j)$ needs to be computed and not the mapping φ . After replacing the inner product with the kernel in Eq. (13), the solution for f is as follows:

$$f(x) = \sum_{i=1}^L \alpha_i k(x_i, x) + b \quad (16)$$

There are number of kernels that can be used in Support Vector Machines models. These include, for example, Linear, Polynomial, Radial Basis Function (RBF), and Sigmoid. The RBF is by far the most popular choice of kernel types used in Support Vector Machines, due to its high performance. The non-linear radial basis function kernel is defined by Eq. (17) [21]:

$$k(x_i, x_j) = e^{-\frac{\|x_i - x_j\|^2}{2\sigma^2}} \quad (17)$$

where $\|x_i - x_j\|^2$ is the squared Euclidean distance between two feature vectors namely, x_i and x_j , σ is a parameter of the Gaussian RBF which defines the width of the ‘bell’ curve. In order to choose the optimal parameter configuration, we perform Cross Validation (CV) on the training data using grid-search. The grid search considers a range of values for each parameter configuration and the best parameter configuration is the one that offers the lowest cross validation error. K -fold cross validation is used. In K -fold CV, the training data points are randomly partitioned into k equal-sized parts. $k-1$ parts are used for training and the remaining part for

validation, considering all different permutations. We estimate the cross-validation error by averaging the errors that are obtained from each permutation.

2.2. Solar PV electricity production on rooftops

Yearly mean solar radiation for the rooftops of more than 10,000 buildings (city scale) has been estimated, using fine resolution LiDAR point data, by SITG (Le système d'information du territoire à Genève) [32,33] and is freely accessible from <http://ge.ch/sitg/>. We used solar radiation analysis tools in Geographic Information System (GIS), in combination with MATLAB, to model solar potential on building roofs at building and neighbourhood scales to verify the city-scale solar model provided by SITG. Fig. 2 shows a visualisation of the solar potential availability on the rooftops in three different scales, namely building scale (Fig. 2a), neighbourhood scale (Fig. 2b), and city scale (Fig. 2c). The solar PV electricity potentials for rooftops have been estimated as follows: (i) LiDAR point data are used to make a Digital Surface Model (DSM) with precision of $0.5 \text{ m} \times 0.5 \text{ m}$ which includes buildings with their different roof shapes as well as details on the landscape. (ii) DSM is then used to extract the roof area, slope, aspect, and orientation of roof surfaces which will be used in the calculation of solar potential. (iii) The average 20 years meteorological data (e.g. solar radiation, cloud cover, temperature) from 1980 to 2000 is obtained from Meteonorm (<http://www.meteonorm.com/>) in order to estimate the solar radiations components (direct-beam, sky-diffuse, and ground reflected) on the tilted surfaces. (iv) The calculations of solar radiation components are performed in MATLAB using Hay anisotropic model for sky-diffuse radiation [34,35]. (v) Shading co-efficient on the direct and diffuse radiation components is taken into account [32,33]. (vi) Useful roof areas for PV installation are defined using the following thresholds: (a) the superstructures from roof surfaces are removed; (b) only surface having mean solar radiation $\geq 1000 \text{ kWh/m}^2$ are considered [7,36]; (c) a 1-m-buffer is generated

around each remaining roof surface [10]; (d) only roof areas larger than 5 m^2 are considered, the minimum useful areas obtained after applying thresholds a, b, c; (vii) The energy output, that is, the maximum potential of solar PV electricity production on the rooftops is estimated through multiplying the annual mean solar radiation (GWh/year) and the useful roof area for PV installation, taking into account the average efficiency (20%) and the 79% performance ratio for mono-crystalline PV panels (<http://ge.ch/sitg/>).

3. Roof characteristics and solar potential

We analysed the roofs in terms of slopes and facing directions or aspects for all available buildings of the city of Geneva (Fig. 2c). We also analysed the mean annual solar radiation received by the roofs as a function of roof slope and aspect (Fig. 3). Considering first the slope, the results show that the most common roof slopes are in the sectors of $10\text{--}20^\circ$ and $30\text{--}40^\circ$, with the sector of $20\text{--}30^\circ$ being a close second (Fig. 3a). Generalising, we show that slopes between 10° and 40° are by far the most common in the city of Geneva. Conversely, slopes in the range $70\text{--}80^\circ$ are rare, and so are slopes in the ranges $60\text{--}70^\circ$ and $0\text{--}10^\circ$. The latter represents flat roofs, which are thus comparatively rare in Geneva.

The effect of roof slope on received annual solar radiation is shown in Fig. 3b. The results show that the flat to gently sloping roofs, those sloping $0\text{--}40^\circ$, receive the greatest solar radiation. In fact, there is a clear inverse relationship between roof slope and received solar radiation: the greater the slope the less the received radiation. Thus, the steepest sloping roofs, with slopes of $70\text{--}80^\circ$, receive the least amount of solar radiation.

Considering next the roof aspect, the results show that south-facing roofs are the most common, followed by roofs facing either southeast or southwest (Fig. 3c). As expected, the roofs facing south receive the greatest solar radiation (Fig. 3d). These are followed by roofs facing west and east, with the roofs facing northwest, northeast and, in particular, north receiving the least radiation, as

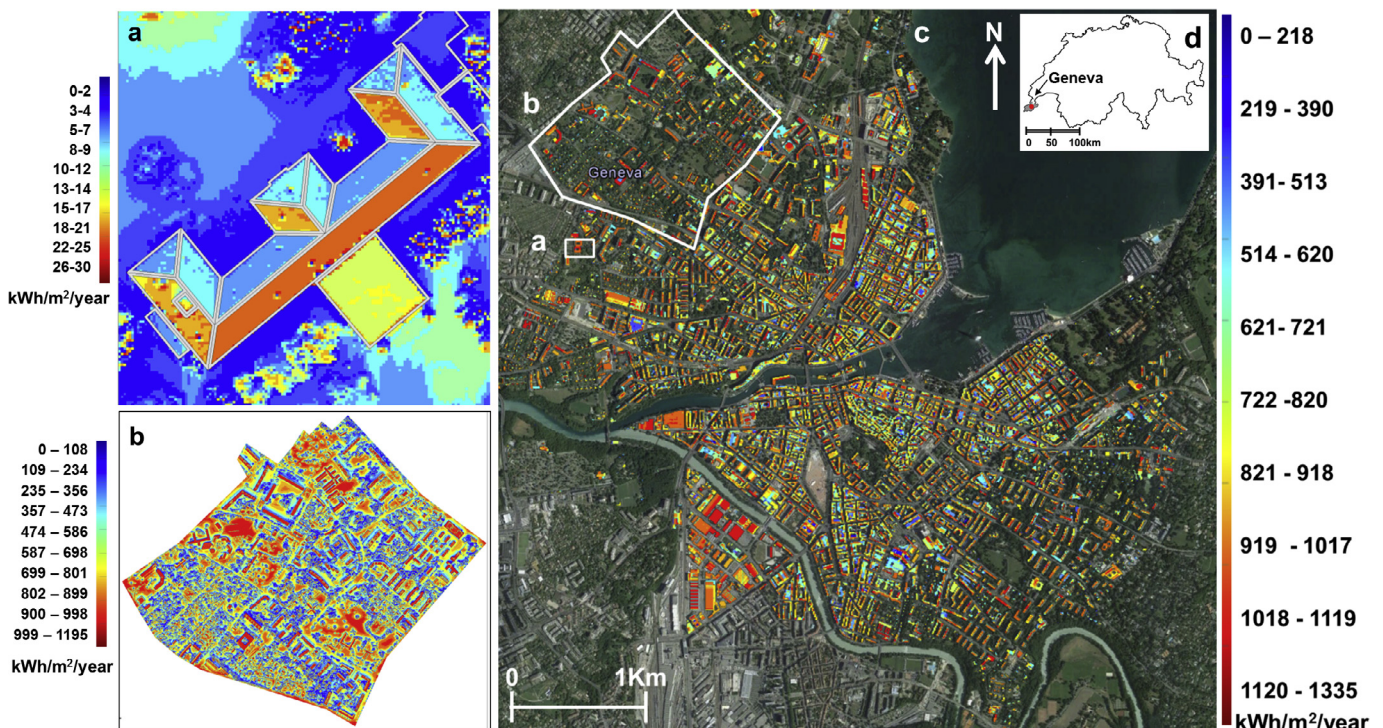


Fig. 2. Yearly mean solar radiation of building roofs in the city of Geneva at three different scales, namely (a) a building scale, (b) a neighbourhood scale, and (c) a city scale.

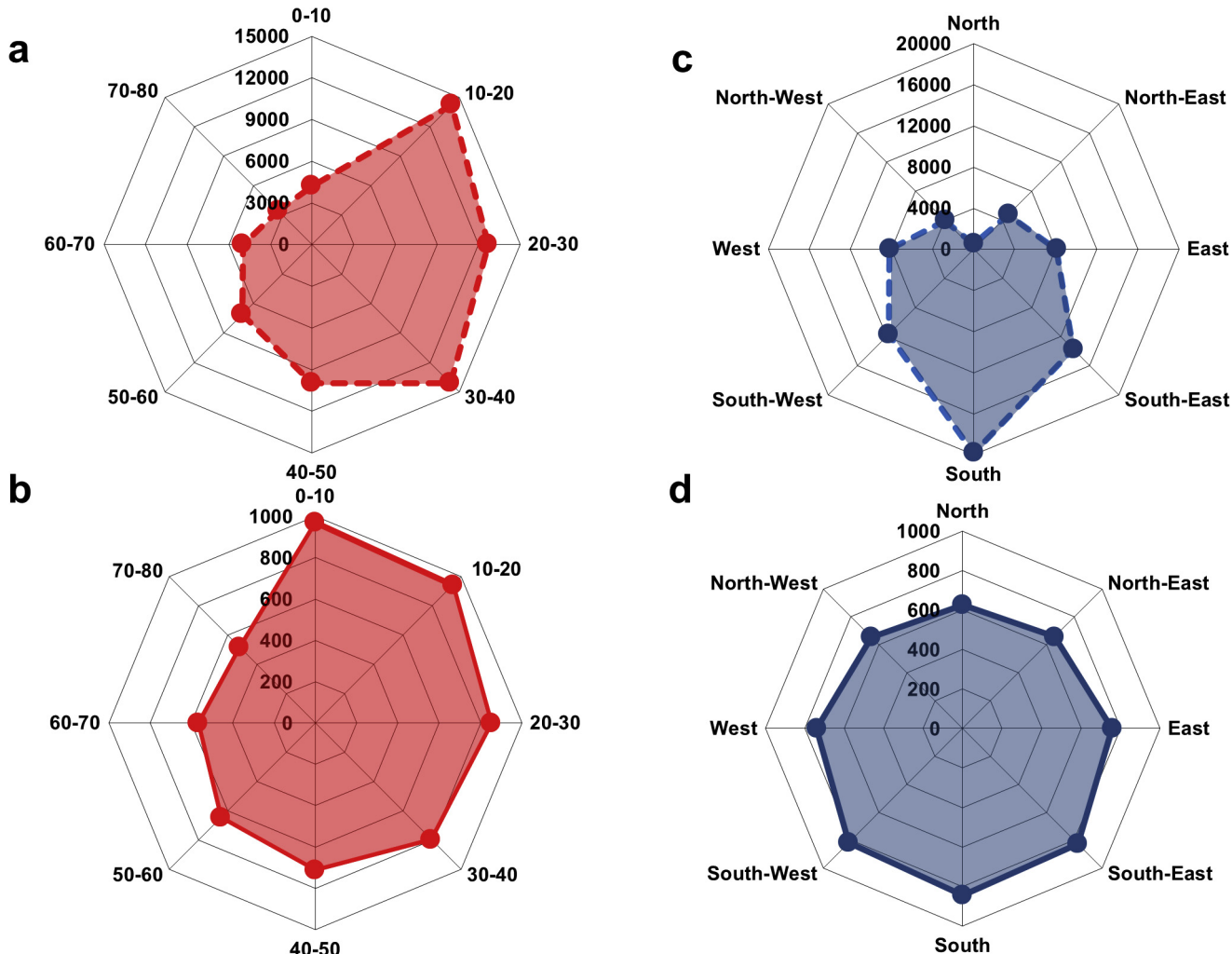


Fig. 3. Number of building roof surfaces for different ranges of (a) slope and (c) aspect. Annual mean solar radiation (kWh/m^2) of roof surfaces for different ranges of (b) slope and (d) aspect.

expected.

These results can now be combined so that the monthly and yearly received solar radiations are shown as functions of both roof slope and aspect or facing direction (Fig. 4). In Fig. 4a and b we show monthly and annual mean solar radiation (kWh/m^2) for a typical neighbourhood in Geneva (see Fig. 2b for the location of neighbourhood). In Fig. 4c we only show the annual mean solar radiation (kWh/m^2) as a function of slope and aspect of the roof surfaces for all the studied buildings in the city of Geneva. The illustrations demonstrate very well the following principal result: Fig. 4a shows that in winter only south-facing and inclined roofs (with slopes up to 40°) get high values. On approaching summer the gently sloping roofs become more favourable and the potential more equally distributed over all aspects. In June and July, roofs with slopes up to $30\text{--}40^\circ$ reach almost the same solar radiation irrespective of orientation (aspect). Fig. 4b and c show that the most favourable surfaces have a slope of up to 40° and an aspect between southeast, south and southwest. Remarkably, for north-facing roofs with gentle slopes the potential is not that much different from gently sloping east and west oriented roofs. The steeper the slope, the lower the values for annual radiation although for southeast and southwest aspects, even roofs with slopes up to 70° get radiation values of $800 \text{ kWh}/\text{m}^2$ and more.

Several studies for Geneva [37,38], and generally for Switzerland

[39], show that a tilt angle between 30° and 40° is commonly considered as optimal roof slope for installing solar panels. For example, for the city of Zürich, located at latitude 47°N , an optimum angle of 30° for the tilt of the roof is reported by Ref. [39]. Similarly, for the city of Geneva, located at latitude 46°N , the optimal tilt angle for installation of PV on rooftops is regarded as 30° [37,38]. The knowledge of the optimum tilt angle is very important in order to obtain the highest possible annual or seasonal solar energy yield. There have been several studies analysing the correlation between the optimal angle for a fixed Building Integrated Photovoltaic (BIPV) system and the latitude of the system's site. For example, Chen et al. [40] suggests using only the latitude angle for the tilted panel. Several other studies, however [41,42], show that the annual and seasonal optimum tilt angle depends on not only the latitude of the site, but also the weather conditions (e.g. seasonal weather patterns such as winter clouds) as well as surrounding obstacles, providing shading in urban areas. Several studies indicate the annual optimum tilt of a PV panel is never greater than the site latitude, but can be up to 10° less than the latitude. More specifically, a tilt angle equal to the site latitude is optimal for an ideal and totally clear skies throughout the year. For different seasons of the year, however, the optimum tilt varies by up to 15° from that of the site latitude (more in the winter, less in the summer).

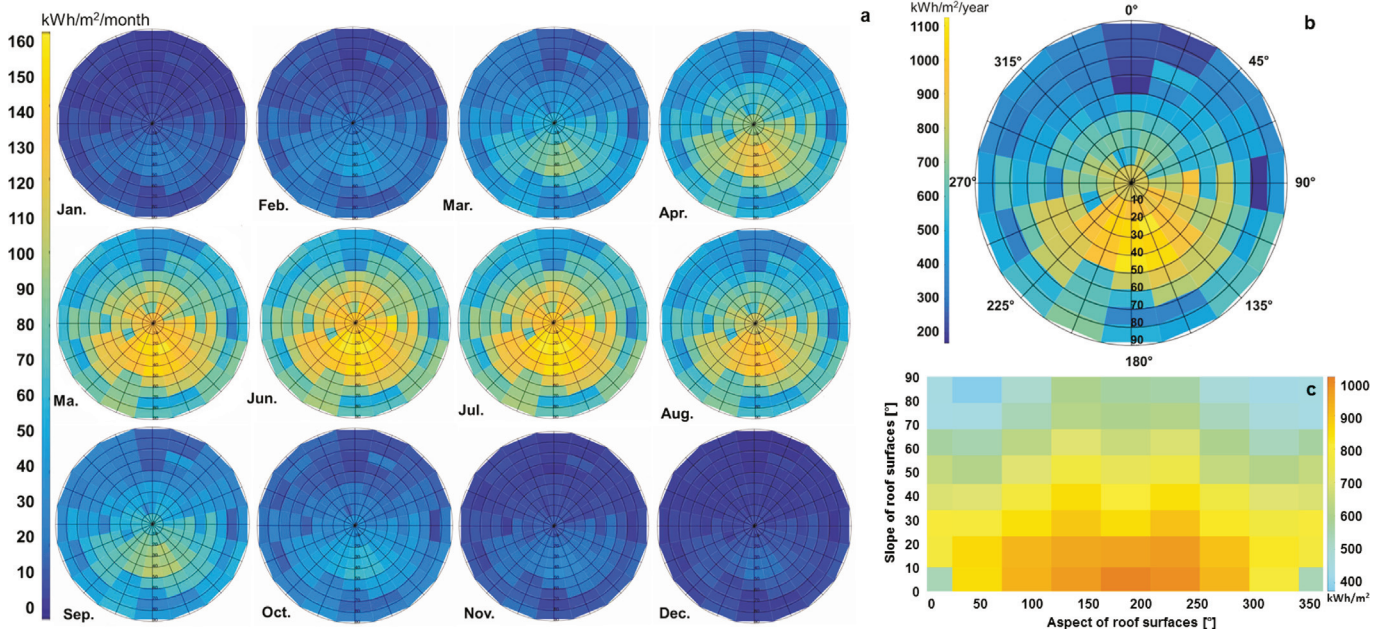


Fig. 4. (a) Monthly and (b) annual mean solar radiation (kWh/m^2) as a function of slope and aspect of roof surfaces for a typical neighbourhood, located in Fig. 2b, and (b) annual mean solar radiation (kWh/m^2) as a function of slope and aspect of roof surfaces for buildings in the entire city of Geneva (Fig. 2c).

4. Roof-shape classification

The total number of buildings chosen and classified for this study of the city of Geneva is 10,085. Exploration of the buildings shows that, for Geneva, the roofs fall into 13 shapes (Fig. 5), namely flat, shed, gabled, hipped, gambrel, mansard flat, mansard hipped,

cross-hipped, cross-gabled, corner-hipped, corner-gabled, pyramidal, and complex – the last one being a hybrid or mixture of several of the above roof shapes. Some of these 13 roof shapes, however, are not easy to classify properly and use in practice. For the purpose of the present analysis, we have thus divided the above 13 roof shapes into 6 main roof-shape classes, which are flat and shed,

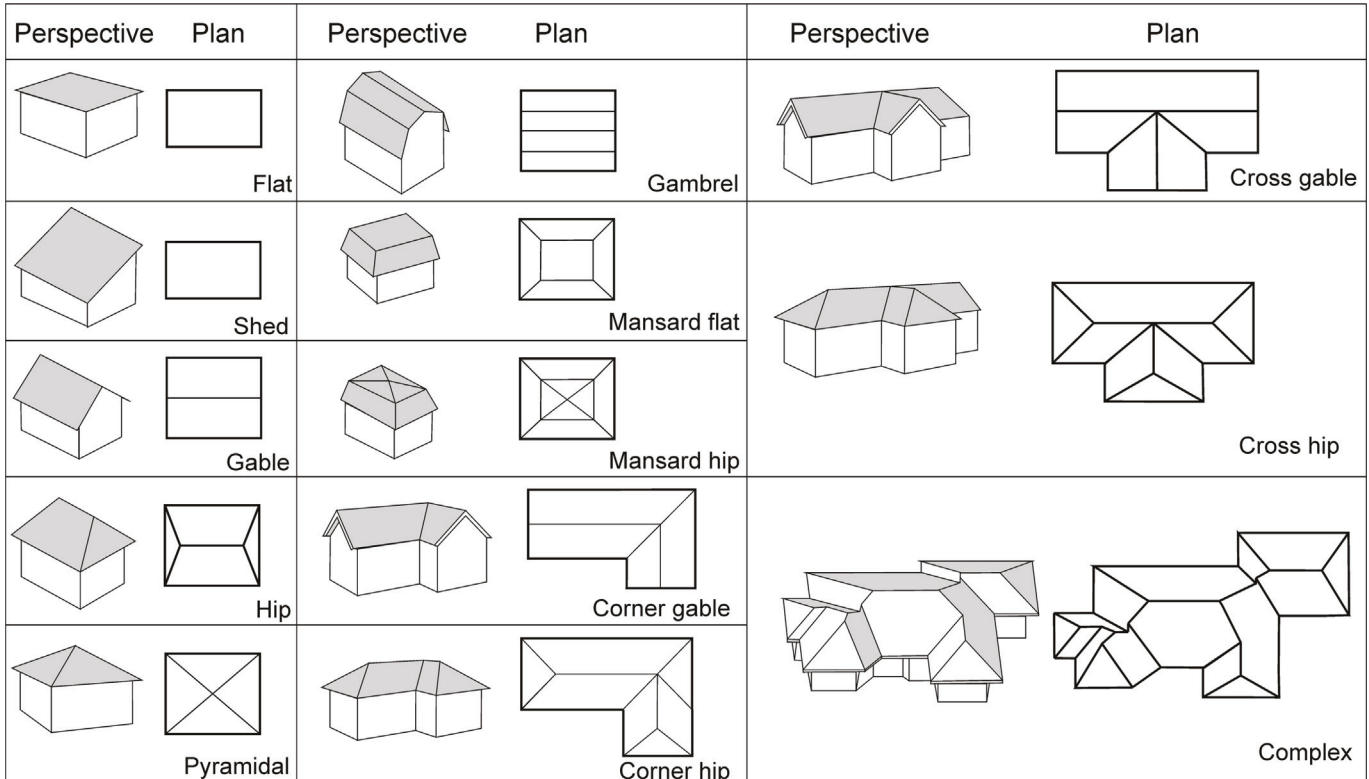


Fig. 5. Schematic presentation of the most common roof shapes (perspective and plan view) of the buildings in the city of Geneva.

Table 1

Schematic presentation of different roof-shape classes.

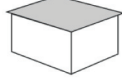
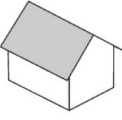
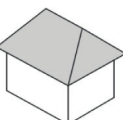
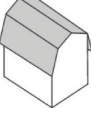
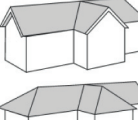
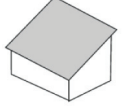
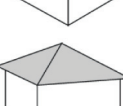
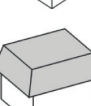
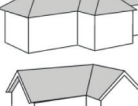
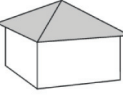
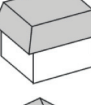
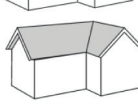
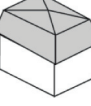
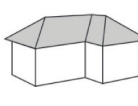
Roof classes					
Flat & Shed	Gable	Hip & Pyramidal	Gambrel & Mansard	Cross and corner Gable & Hip	Complex
0	1	2	3	4	5
					
					
					
					

Table 2

The description of 35 features used in the feature selection when classifying roof shapes.

Number (35 features)	Feature type description
1	Number of roof surfaces for each building
9	Slope distribution (10° bin width) from 0 to 90°
9	Percentage of total roof area for each roof slope category
8	Aspect distribution (45° bin width) from 0 to 360°
8	Percentage of total roof area for each roof aspect category

gabled, hipped, gambrel and mansard, cross/corner hipped and gabled, and complex (Table 1). We then apply the Support Vector Machines algorithm (SVMs) for classifying the roof shapes, using the following steps (a to d).

- (a) **Feature selection.** We select the following 5 feature types for the roof shapes (Table 2): (a) Number of roofs facing given directions, or roof aspects (bin width 22.5°, from 0 to 360°). (b) Number of roofs with given surface slopes (bin width 10°, from 0 to 90°). (c) Number of roofs with given roof shapes. (d) Percentage of total roof area within a certain slope range (bin width). (e) Percentage of total roof area within a certain aspect range (bin width). Altogether, there were 35 features or parameters were selected. These features are listed in Table 2.
- (b) **Scaling of the dataset.** Each feature is normalised by subtracting its mean and dividing the result by the standard deviation. The features in the labelled data are also scaled.
- (c) **Data labelling.** A labelled data (data where the classes are known) is used to train and test the classifier using SVM. The classifier is then applied to the rest of the data. Since no labelled data exist for shapes of the roofs of Geneva, we manually label the data. In this step, a total of 717 buildings (some 6% of total data) were manually labelled using Google Earth and, in particular, a high-quality aerial map from Swisstopo (<https://map.geo.admin.ch>). Examples of labelling roof shapes using high resolution aerial photographs of roofs for different classes are shown in Fig. 6. The number of labelled buildings for each roof type is as follows. Flat: 127,

gabled: 127, hipped: 124, gambrel and mansard: 118, cross and corner hipped and gabled: 115, complex roofs: 106; Table 3). SVM was then used to classify the roof shapes for the rest of the buildings (9368).

(d) SVM testing and training.

- For the purpose of testing and training, the labelled data are divided into two unequal parts: 75% for training and cross-validation and 25% for testing the classifier (Table 3).
- Radial Basis Function (RBF) kernel is used to perform the SVM classification within Python, using the scikit-learn library [43] and it offers the greatest accuracy.
- Cross-validation is used to assess how the training dataset can be generalised to an independent dataset. K-fold cross-validation (the original sample is randomly partitioned into K equally-sized subsamples) is used in this study. We choose K = 6 which is regarded as a common value.
- SVM classifier from the above step is used to predict the roof shapes for the rest of the buildings of Geneva.
- Classification accuracy metric is used to evaluate the performance of the classifier. The accuracy metric is defined as Eq. (18):

$$\text{accuracy} = \frac{\psi}{\Omega} * 100\% \quad (18)$$

where ψ is the number of correctly classified roof shapes and Ω is the total number of roof shapes.

5. Results

Our results indicate that the SVM classifier is able to identify the 6 types of roof shapes, that is, flat, gable, hip, gambrel & mansard, cross/corner gable & hip, and complex roofs, on average, in 66% of cases (Table 4). The number of testing data and the accuracy of the classification for each of the 6 roof-shape classes is given in Table 4. The aim is to maximize the diagonal numbers of the table (marked in bold) as it means that buildings belonging to the class 0 (flat & shed), for example, are correctly classified as part of class 0. Also, 2 out of 32 flat & shed roof shapes are misclassified as complex. Thus, the obtained accuracy for the flat roof-shape is 94%. The results in

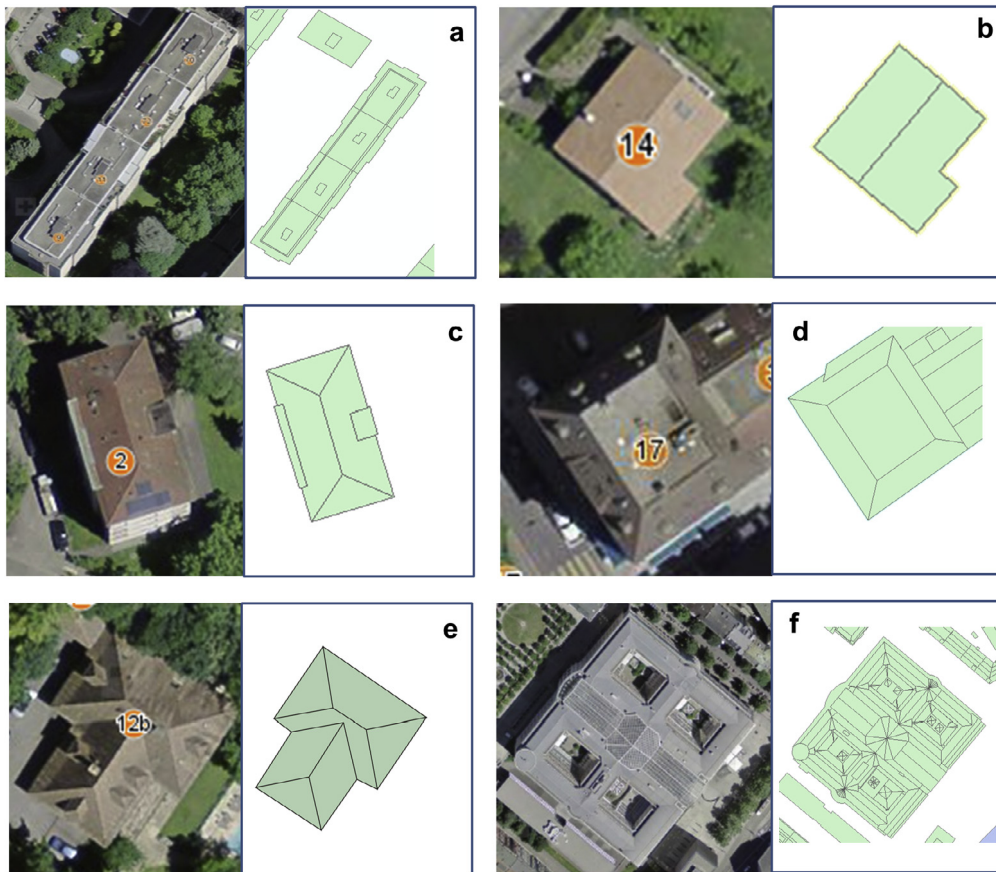


Fig. 6. Examples of labelling roof shapes using high resolution aerial photographs of roofs for different classes. For each shape class, the aerial photograph is on the left, the labelled roof shape on the right. (a) Flat roof (class 0). (b) Gable (class 1). (c) Hip (class 2). (d) Mansard (class 3). (e) Cross/corner Gable and Hip (class 4). (f) Complex (class 5).

Table 4 indicate that, on average, flat and complex roofs are classified more accurately than the other types. The worst accuracy belongs to the hip & pyramidal roofs in which many are misclassified as gable roof due to their similar characteristics.

After the validation, the classification is applied to the rest of data. Distribution of the various classes of roof shapes in Geneva as a whole is shown in Fig. 7. While the flat & shed are very common,

the complex roof shapes (red) are very extensive. To get more detailed information about the roofs, it is not enough just to look at entire roofs, whose spatial distribution and numbers are shown in Fig. 7, but also at the individual parts or surfaces of which the roofs are composed. Thus, we distinguish here between the roofs themselves, the number of roofs being equal to the number of buildings (a total of 10,085 analysed), and the surfaces that

Table 3

Total number of labelled data for each roof-shape class/group, training data for each roof-shape class (75% of total labelled data), and testing data for each roof-shape class (25% of total labelled data).

Class	Flat & Shed	Gable	Hip & Pyramidal	Gambrel & Mansard	Cross and corner Gable & Hip	Complex
Total number of labelled data	127	127	124	118	115	106
Training data	95	95	93	89	86	80
Testing data	32	32	31	29	29	26

Table 4

The results of the accuracy matrix for testing data for each roof -shape class (66% overall accuracy). The diagonal numbers of the table (marked in bold) means that buildings belonging to the class i are correctly classified as part of class i.

Testing data	Flat & Shed	Gable	Hip & Pyramidal	Gambrel & Mansard	Cross and corner Gable & Hip	Complex	Accuracy for each class (%)
	0	1	2	3	4	5	
0 (32)	30	0	0	0	0	2	94
1 (32)	4	18	6	4	0	0	56
2 (31)	0	8	15	4	3	1	48
3 (29)	1	2	4	18	4	0	62
4 (29)	2	0	5	2	15	5	52
5 (26)	1	0	0	2	1	22	85

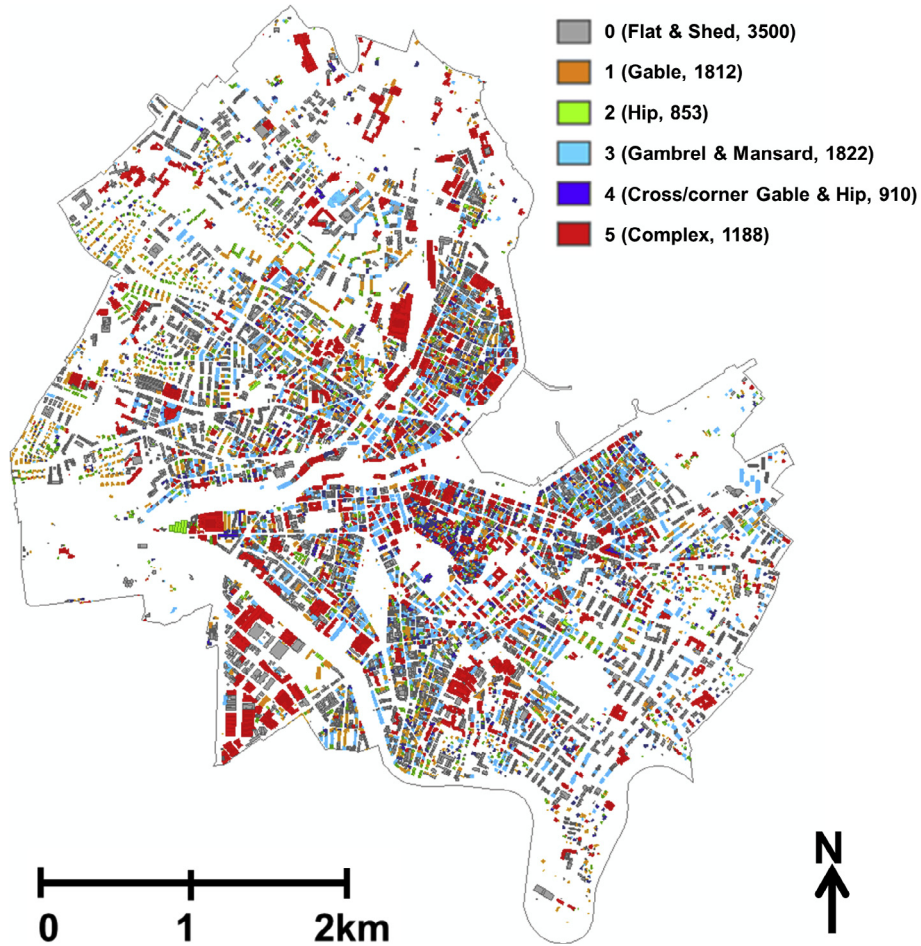


Fig. 7. Results of roof-shape classification for building data in the city of Geneva. The colours show distribution of different roof-shape class for a total of 10,085 buildings in the city of Geneva.

constitute the roofs. More specifically, the number of roof surfaces (in parentheses) that belong to each roof shape is as follows (Fig. 8): flat and shed (11,521), gable (4411), hip (3696), gambrel an mansard (13,529), cross/corner (7252), and complex (26,1002). The total number of analysed roof surfaces is thus 66,811.

In Fig. 8 the number of roof surfaces is plotted against roof slope (Fig. 8a) and against roof aspect or facing direction (Fig. 8b). There are various points that can be inferred from Fig. 8a. The first is that surfaces belonging to complex roofs are the most common for all the slopes, except the steepest ones. This is partly a reflection of the comparatively high number of complex roof surfaces in general (26,102 or 39% of the total). Partly, however, this fact reflects the geometry of the complex roofs which tend to have roof surfaces of a greater variety of slopes than the other shapes (Figs. 5 and 6). The complex roofs generally belong to buildings with complex shape and large surface roof area. These include museums, railway stations, and churches. A second point is that the flat & shed roof class includes surfaces that slope as much as 80°. This is primarily because the flat roof class includes also the shed roofs, many of which have steep slopes. The third point is that there are some surfaces sloping in excess of 80°. These are included here (and in Fig. 4) for the sake of completeness, but were omitted for the results presented in Fig. 3.

As for the direction of facing or aspect of roof surfaces, the

results agree with those obtained for the entire roofs (Figs. 3 and 4), namely that most of roof surfaces face in a southerly direction (Fig. 8b). More specifically, the aspect peak is roughly at the azimuth of 160–200°, that is, from south-southeast through south to south-southwest.

In order to analyse the solar PV potential of buildings, we need to calculate the available or useful roof areas of the buildings for PV installation. This we did by removing the superstructures from the roofs, as well as 1 m² from the margin of roof surfaces, and considering the 28 m² threshold (only areas larger than 28 m² are considered) for roofs due to the size of a typical PV panel (Fig. 9) [10]. The resulting available area is always smaller than the total roof area (Fig. 10). In addition, footprint areas are widely available so that the available roof areas can also be compared with the corresponding footprint areas.

Because of the wide availability of footprint areas, we also calculated the ratio of useful roof area for each type of roof shape to that of the corresponding building footprint area. The results show that for most roof shapes this ratio is close to one (Fig. 11). The only exceptions, and those are not great, are the hip (ratio of 1.10) and gable (ratio 1.18). The results thus suggest that the footprint area can be used as a measure of the useful roof area for the installation of PVs.

Once the useful area has been calculated, the potential PV

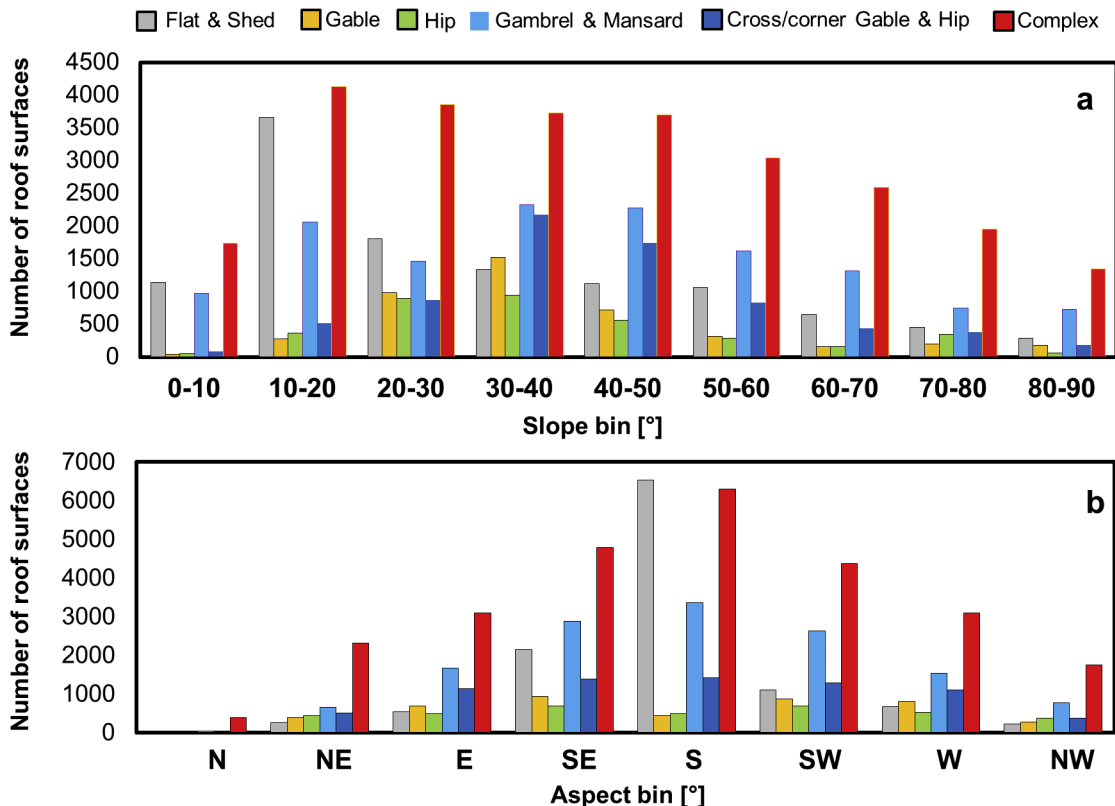


Fig. 8. Frequency distribution of roof surfaces versus (a) roof slope and (b) aspect for different roof-shape groups. The number (in parentheses) of roof surfaces are as follows: flat and shed (11,521), gable (4411), hip (3696), gambrel and mansard (13,529), cross/corner (7252), and complex (26,102). The total number of analysed roof surfaces is thus 66,811.

potential for the various roof shape groups could be estimated. Here we did so by calculating the received mean solar radiation (kWh/m^2) and the PV potential (MWh/year; solar electricity production per year) for each of the 6 main roof shape groups ($1 \text{ kWh} = 3.6 \times 10^6 \text{ J}$; $1 \text{ MWh} = 3.6 \times 10^9 \text{ J}$). The results (Fig. 12a) show the flat & shed roofs having the highest received mean solar

radiation of 809 kWh/m^2 . This high value is followed by somewhat lower values for cross/corner (806 kWh/m^2) and hip (800 kWh/m^2). Somewhat lower than these are the received radiation by gambrel and mansard (789 kWh/m^2), followed by the considerably lower values for the complex (761 kWh/m^2) and the gable (744 kWh/m^2) roofs.

Since received mean solar radiation is second lowest for complex roofs, it may come as a surprise that they have by far the greatest average PV potential in Geneva (Fig. 12b). The reason is that complex roofs have the greatest number of roof surfaces (Fig. 8), the largest cumulative roof area and available or useful roof area for PVs (Fig. 10). Following the complex roofs in terms of solar PV potential are the flat & shed roofs (Fig. 12b). This is less surprising since these have the highest annual mean solar radiation per unit area (Fig. 12a). The other roof shapes, namely gable, hip, gambrel & mansard, and cross/corner have similar PV potential, the gable being the lowest.

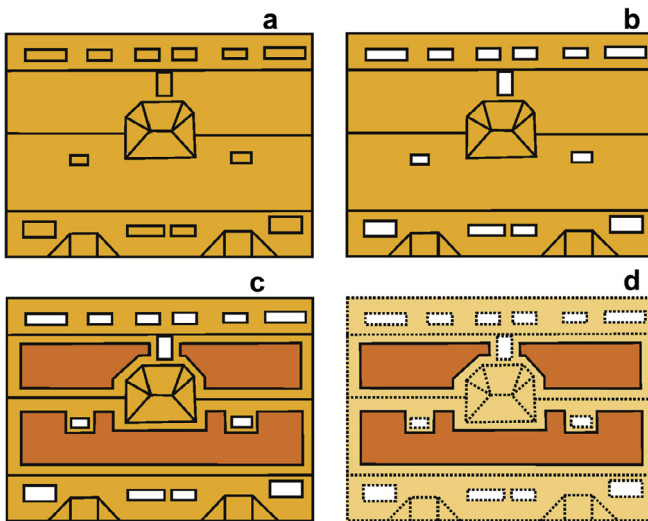


Fig. 9. Schematic presentation of different steps taken to estimate available roof area for a building. (a) A building with detailed roof surfaces including superstructure (e.g., a chimney, dormers, and a staircase). (b) Removal of the superstructures from roof surfaces. (c) Creation of a 1 m² buffer around each remaining roof surface. (d) The final available roof useful area for PV installation after removing the areas less than 28 m².

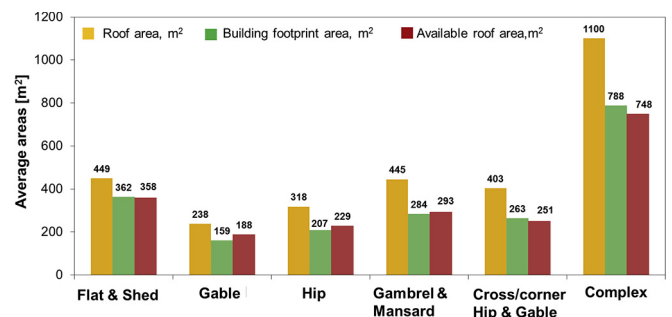


Fig. 10. Average roof area (m²), average building footprint area (m²), and average available roof area (m²) for PV installations for different roof-shape classes.

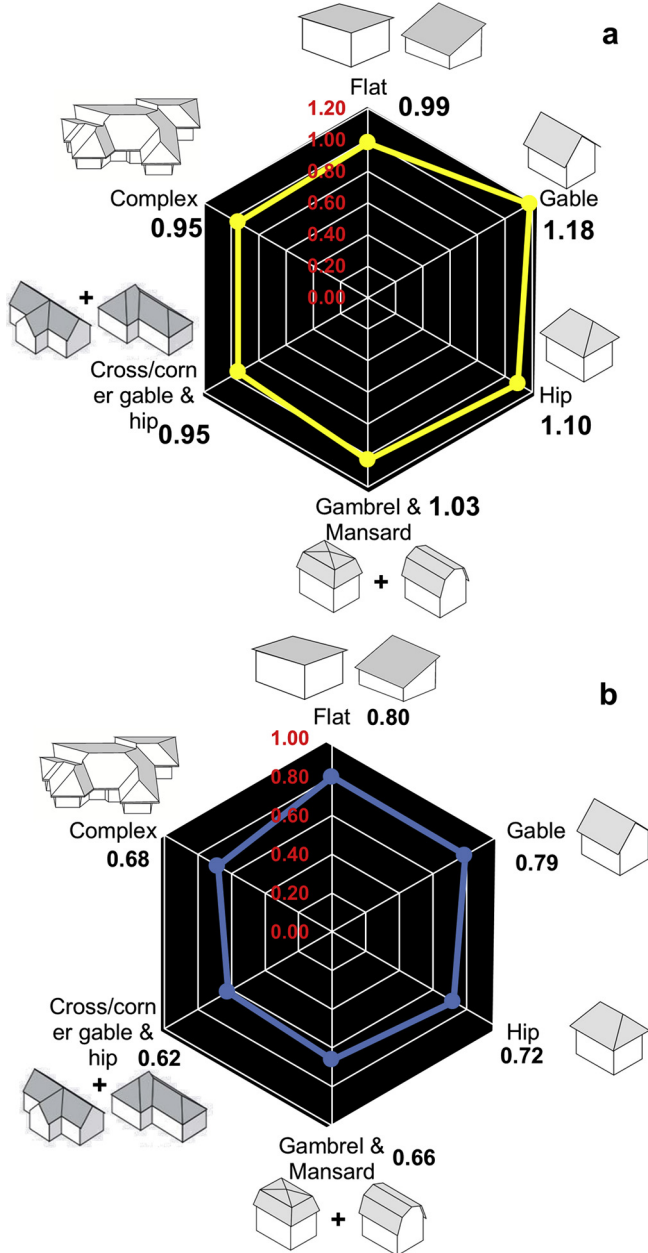


Fig. 11. (a) Ratio of available or useful roof areas for PV installations to footprint areas of buildings in different roof-shape groups. (b) Ratio of useful roof areas to the roof areas considering the slope of each roof surface.

6. Discussion and conclusions

The present study shows that the machine-learning technique can be very useful in classifying roof shapes for city scale, as demonstrated here for the city of Geneva. By implication, the same method can be extended to include larger cities and, eventually, entire countries [44], as well as other European countries. The results of the study are particularly useful for designers, investors, owners, and stockholders in providing quantitative information on the effects of roof shape on the PV solar potential at the design stage. The results are also important from planning and policy-making perspectives in that they provide helpful input for choosing the right type of roof when retrofitting existing buildings or designing new buildings. The classification of roofs based on

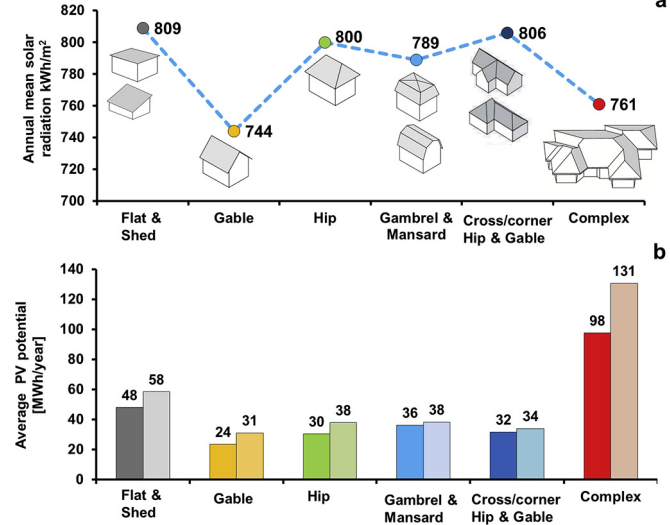


Fig. 12. (a) Received annual mean solar radiation in kWh/m² and (b) average PV potential for different roof-shape groups. In figure b, the darker colours for each roof-shape group show the estimated average PV potential based on the total solar radiation received by the roof surfaces. By contrast, the lighter colours show the estimated average PV potential based only on the solar radiation in excess of 800 kWh/m² received by the roof surfaces. (For interpretation of the references to colour in this figure legend, the reader is referred to the web version of this article.)

their useful area for PV installations and potential for receiving solar energy should encourage policy makers and investors to select roof design and construction that (i) maximizes the possibility of mounting solar panels on roofs, (ii) provides greater capacity for solar energy per building and (iii) lowers installation cost due to simplification of the installation.

A further development of the concepts and methods presented here is not only to look at the roof shapes and their potential for PV installations, but also to consider what the buildings are used for. While we do not propose to go deeply into these aspects here, as an indication of this further development of the present methods, we have explored the main uses of the buildings in relation to their roof shapes and the associated PV potential (Fig. 13).

The buildings in Geneva are grouped according to the following building types (<http://ge.ch/sitg/>): mixed, activity, residential, collective, and others. (1) Mixed buildings are those that function partly as residential and partly as commercial. These include, for example, buildings where family flats are on the first and/or second floor but shops on the ground floor. (2) Under the term activity we include commercial stores, offices, hotels, restaurants, and buildings or spaces for industry. (3) Residential covers the buildings where people live – their homes. (4) Collective denotes those buildings used for educational and cultural purposes as well as for health and sport. (5) Others are buildings that do not fit into one of the previous four categories.

The results (Fig. 13a) show that residential building types are the highest percentage of buildings for flat & shed, gable, and hip, whereas mixed buildings are the highest percentage for gambrel & mansard, cross/corner hip & gable, and complex buildings. For those roof-shape groups where residential is highest, mixed is the second highest, while residential is the second highest percentage for those shape groups where mixed is the highest percentage. Clearly, residential and mixed together dominate and jointly range from 54% for complex shapes to 75% for hip.

In terms of contribution to the total solar PV potential in the shape classes, the picture is somewhat different (Fig. 13b). While residential is the highest percentage (44%) for gable and hip, and

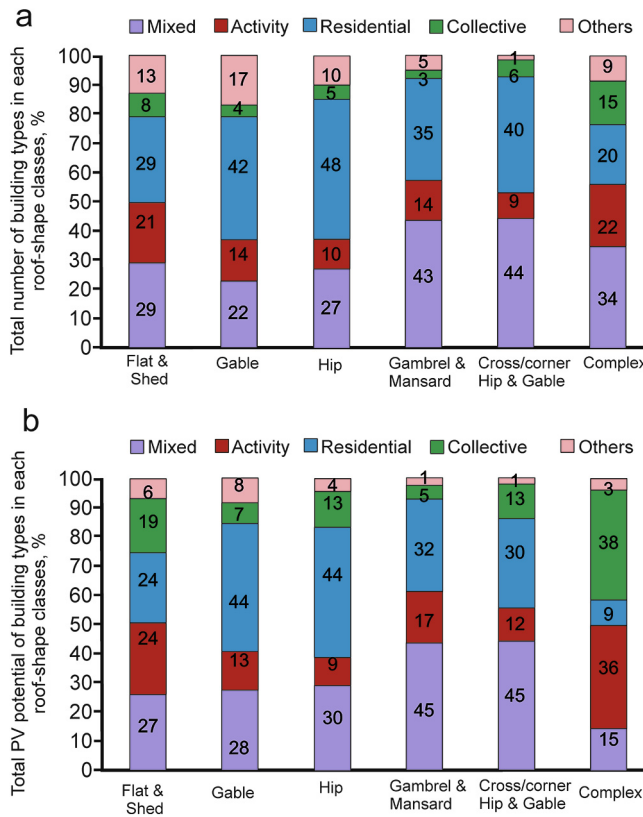


Fig. 13. Roof-shape classes versus building types (building activity) and solar PV potential. The building types are: (1) Mixed, which are partly used as residential and partly as commercial. (2) Activity, where the use includes functions as commercial stores, offices, hotels, restaurant, and industrial functions. (3) Residential, where the buildings function only as family homes. (4) Collective, where the use is for educational, cultural, and health and sport purposes. (5) Others, where the buildings are primary for parking or function as transport infrastructures. (a) Total number of buildings of the above types given as percentage of all the buildings for a given roof shape. (b) Total PV potential for the building types given as percentage of all the buildings for a given roof shape.

mixed for gambrel & mansard and cross/corner (45%), collective is the highest percentage for buildings with complex roof shape (38%), and mixed is highest for flat and shed (27%). For flat & shed, however, three of the building activity types make a very similar contribution to the solar PV potential, namely mixed, activity, and residential. Clearly, the contribution of the building types to the solar PV is somewhat complex and further studies on this topic may be of interest.

There are other possibilities for expanding and developing the work presented here, with a view of providing input and help for urban design, aiming at PV installations on the roofs, in the future. For example, the roof-shape classification could be refined, adding more roof shapes into account. In Fig. 5 we list 13 roof shapes, which are then reduced to the 6 shape classes used in the present paper. While we do not think that it is realistic to try to use all the 13 shapes, a more refined classification, with more than 6 main groups, would allow us to explore finer aspects of the variation in roof shapes in cities, as well as their solar PV potential. Another aspect is to try to use a more adapted machine learning algorithm (e.g. Random Forests) and expand the classification of roof shapes to the national scale. It is also important to improve the training of the machine learning procedure so as to get higher percentage of correct identification of the roof shapes. Presently, the SVM correctly identifies the 6 main roof shapes in 66% of the cases. While this is certainly acceptable, with further refinement and

training on new and different data the success rate may increase in this respect.

In conclusion, in this paper we show that machine-learning approach through the Support Vector Machine classification is a promising method for classifying roof shapes. We use 6 main roof shape classes and rank them based on their useful areas for PV installations. We also show that for most of the roof shapes the ratio between the useful roof area and the building footprint is close to one. Since footprint areas are widely available, this result is very important since it suggests that footprint areas can be used as approximate substitutes to assess useful roof areas for PVs. We conclude that the solar roof shape classification provides basic information that should be of help in designing new buildings, retrofitting innovations on the building roofs, as well as for efficient solar integration on roofs.

Acknowledgments

This research has been financed partly by CTI (Commission for Technology and Innovation) within SCCER FEEB&D (CTI.2014.0119) and partly by Swiss National Science Foundation under Mobility Fellowship P300P2 174514.

References

- [1] L. Wigington, H. Nguyen, J. Pearce, Quantifying rooftop solar photovoltaic potential for regional renewable energy policy, *Comput. Environ. Urban* 34 (2010) 345–357.
- [2] S. Nowak, M. Gutschner, D. Ruoss, P. Togweiler, T. Schoen, Potential of Building Integrated Photovoltaics. Report IEA-PVPS T7–4, 2002.
- [3] J. Goodling, R. Crook, A.S. Tomlin, Modelling of roof geometries from low-resolution LiDAR data for city-scale solar energy applications using a neighboring buildings method, *Appl. Energy* 148 (2015) 93–104.
- [4] F. Tarsha-Kurdı, T. Landes, P. Grussenmeyer, M. Koehl, Model-driven and Data-driven Approaches Using LiDAR Data: Analysis and Comparison, Munich, 2007, pp. 87–92.
- [5] M.C. Brito, N. Gomes, T. Santos, J.A. Tenedorio, Photovoltaic potential in a Lisbon suburb using LiDAR data, *Sol. Energy* 86 (2012) 283–288.
- [6] C. Carneiro, E. Morello, G. Desthieux, . Assessment of Solar Irradiance on the Urban Fabric for the Production of Renewable Energy Using Lidar Data and Image Processing Techniques, *Advances in GIScience* Springer, 2009, pp. 83–112.
- [7] N. Mohajeri, A. Gudmundsson, G. Upadhyay, D. Assouline, J. Kämpf, J.L. Scartezzini, Effects of urban compactness on solar energy potential, *Renew. Energy* 93 (2016) 469–482.
- [8] C. Carneiro, E. Morello, T. Voegtle, F. Golay, Digital urban morphometrics: automatic extraction and assessment of morphological properties of buildings, *T. GIS* 14 (2010) 497–531.
- [9] N. Lukac, S. Seme, D. Zlaus, G. Stumberger, B. Zalik, Buildings roofs photovoltaic potential assessment based on (Light Detection and Ranging) data, *Energy* 66 (2014) 598–609.
- [10] D. Assouline, N. Mohajeri, J.-L. Scartezzini, Quantifying rooftop photovoltaic solar energy potential: a machine learning approach, *Sol. Energy* 141 (2017) 278–296.
- [11] J. Goodling, R. Crook, A.S. Tomlin, Modelling of roof geometries from low-resolution LiDAR data for city-scale solar energy applications using a neighboring buildings method, *Appl. Energy* 148 (2015) 93–104.
- [12] M. Kada, Scale-dependent simplification of 3D building models based on cell decomposition and primitive instancing, in: Proceedings of the International Conference on Spatial Information Theory. COSIT'07. Melbourne, Australia, 2007, pp. 222–237.
- [13] J. Khan, M.H. Arsalan, Estimation of rooftop solar photovoltaic potential using geo-spatial techniques: a perspective from planned neighborhood of Karachi – Pakistan, *Renew. Energy* 90 (2016), 188e203.
- [14] S. Izquierdo, M. Rodriguez, N. Fueyo, A method for estimating the geographical distribution of the available roof surface area for large-scale photovoltaic energy-potential evaluations, *Sol. Energy* 82 (2008) 929–939.
- [15] I. Shapiro, The receptivity of roofs to solar panels, in: Proceedings of the 2nd World Sustain. Forum, 1–30 November 2012; Sciforum Electronic Conference Series, vol. 2, 2012.
- [16] E. G. Nault, G. Peronato, Rey M. Andersen, Review and critical analysis of early-design phase evaluation metrics for the solar potential of neighborhood designs, *Build. Environ.* 92 (2015), 679e691.
- [17] D. Li, G. Liu, S. Liao, Solar potential in urban residential buildings, *Sol. Energy* 111 (2015), 225e235.
- [18] K. Konis, A. Games, K. Kensek, Passive performance and building form: an optimization framework for early-stage design support, *Sol. Energy* 125

- (2016) 161–179.
- [19] C. Voyant, G. Notto, S. Kalogirou, M.L. Nivet, C. Paoli, F. Motte, A. Fouilloy, Machine learning methods for solar radiation forecasting: a review, *Renew. Energy* 105 (2017), 569e582.
- [20] M. Kanevski, Statistical learning in geoscience modelling: novel algorithms and challenging case studies, *Comput. Geosci.* 85 (2015) 1–2.
- [21] M. Kanevski, A. Pozdnukhov, V. Timonin, *Machine Learning for Spatial Environmental Data: Theory, Applications, and Software*, EPFL Press, Spain, 2009.
- [22] M. Kanevski, M. Maignan, *Analysis and Modelling of Spatial Environmental Data*, EPFL Press, Lausanne (, 2004).
- [23] C. Cortes, V. Vapnik, Support-vector networks, *Mach. Learn.* 20 (1995) 273–297.
- [24] A. Hur-Ben, J. Watson, A user's guide to Support Vector Machines, *Meth. Mol. Biol.* 609 (2010) 223–239, https://doi.org/10.1007/978-1-60327-241-4_13.
- [25] T. Hastie, R. Tibshirani, J. Friedman, *The Elements of Statistical Learning: Data Mining, Inference, and Prediction*, Springer Series in Statistics, USA, 2013.
- [26] T. Fletcher, *Support Vector Machines Explained*, University College London, 2009.
- [27] C. Burges, A tutorial on support vector machines for pattern recognition, *Data Min. Knowl. Discov.* 2 (1998) 121–167.
- [28] R. Vanderbei, LOQO: an Interior Point Code for Quadratic Programming, Technical Report (Revised) SOR 94-15, Princeton University, 1998.
- [29] V. Vapnik, *Statistical Learning Theory*, John Wiley & Sons, 1998.
- [30] B. Scholkopf, A. Smola, *Learning with Kernels: Support Vector Machines, Regularization, Optimization, MIT Press, Beyond*, 2002.
- [31] A. Smola, B. Scholkopf, A tutorial on support vector regression, *Stat. Comput.* 14 (2004) 199–222.
- [32] G. Desthioux, C. Carneiro, E. Morello, Cadastre Solaire Du Canton De Geneve, Raport final. Etude réalisée par hepia, EPFL et Politecnico di Milano pour le compte du Service de l'énergie-ScanE et des Services industriels genevois (SIG), 2011.
- [33] G. Desthioux, P. Gallinelli, R. Camponovo, Cadastre Solaire Du Canton De Geneve – Phase 2. Analyse du potentiel de production énergétique par les panneaux solaires thermiques et PV. Rapport final. Etude pour le compte de l'Office cantonal de l'énergie (OCEN) et des Services industriels genevois (SIG), 2014.
- [34] D.H.W. Li, T.N.T. Lam, Determining the optimum tilt angle and orientation for solar energy collection based on measured solar radiance data, *Int. J. Photoenergy* (2007), <https://doi.org/10.1155/2007/85402>, 85402.
- [35] D.H.W. Li, G.H.W. Cheung, Study of models for predicting the diffuse irradiance on inclined surfaces, *Appl. Energy* 81 (2005) 170–186.
- [36] D. Robinson, J.L. Scartezzini, M. Montavon, R. Compagnon, SOLURBAN Project: Solar Utilisation Potential of Urban Sites, Swiss Federal Office for Energy, Bundesamt für Energie BFE, Bern (, 2005).
- [37] NET, Nowak Energie & Technologie SA, *Le Potentiel Solaire dans le Canton de Genève*, Technical report, Waldweg 8, Switzerland, St. Ursen, 2004.
- [38] G. Desthioux, P. Gallinelli, R. Camponovo, Analyse du potentiel de production énergétique par les panneaux solaires thermique et PV. Final report. Etude pour le compte de l'Office cantonal de l'énergie (OCEN) et des Services industriels genevois (SIG), Geneva, 2014.
- [39] International Energy Agency (IEA). reportPotential for Building Integrated Photovoltaics. Achievable Levels of Electricity from Photovoltaic Roofs and Façades: Methodology, Case Studies, Rules of Thumb and Determination of the Potential of Building Integrated Photovoltaics for Selected Countries. Summary of Report IEA - PVPS T7–4.
- [40] C.L. Cheng, C.S. Sanchez Jimenez, M. Lee, Research of BIPV optimal tilted angle, use of latitude concept for south orientated plans, *Renew. Energy* 34 (2009) 1644–1650.
- [41] A. Gharakhani Siraki, P. Pillay, Study of optimum tilt angles for solar panels in different latitudes for urban applications, *Sol. Energy* 86 (2012) 1920–1928.
- [42] M. Lave, J. Kleissl, Optimum fixed orientations and benefits of tracking for capturing solar radiation in the continental United States, *Renew. Energy* 36 (2011) 1145–1152.
- [43] F. Pedregosa, G. Varoquaux, A. Gramfort, V. Michel, B. Thirion, O. Grisel, M. Blondel, P. Prettenhofer, R. Weiss, V. Dubourg, J. Vanderplas, A. Passos, D. Cournapeau, M. Brucher, M. Perrot, E. Duchesnay, Scikit-learn: machine learning in Python, *J. Mach. Learn. Res.* 12 (2011) 2825–2830.
- [44] D. Assouline, N. Mohajeri, J.-L. Scartezzini, Building rooftop classification using random Forests for large-scale PV deployment. Earth resources and environmental remote sensing/GIS applications VIII, in: Ulrich Michel (Ed.), Karsten Schulz Proc. of SPIE, vol. 10428, 2017, 1042806, <https://doi.org/10.1117/12.2277692>.